Distinct Genetic Signatures among Pilocytic Astrocytomas Relate to Their Brain Region Origin

Mukesh K. Sharma,[1] David B. Mansur,[2] Guido Reifenberger,[5] Arie Perry,[3] Jeffrey R. Leonard,[4] Kenneth D. Aldape,[6] Meredith G. Albin,[1] Ryan J. Emnett,[1] Simon Loeser,[5] Mark A. Watson,[3] Rakesh Nagarajan,[3] and David H. Gutmann[1]

Departments of [1]Neurology, [2]Radiation Oncology, [3]Pathology and Immunology, and [4]Neurosurgery, Washington University School of Medicine, St. Louis, Missouri; [5]Department of Neuropathology, Heinrich-Heine-University, Düsseldorf, Germany; and [6]Department of Pathology, University of Texas M. D. Anderson Cancer Center, Houston, Texas

Abstract

Pilocytic astrocytomas (PAs) are the most common glioma in children. Whereas many PAs are slow-growing or clinically indolent, others exhibit more aggressive features with tumor recurrence and death. To identify genetic signatures that might predict PA clinical behavior, we did gene expression profiling on 41 primary PAs arising sporadically and in patients with neurofibromatosis type 1 (NF1). Whereas no expression signature was found that could discriminate clinically aggressive or recurrent tumors from more indolent cases, PAs arising in patients with NF1 did exhibit a unique gene expression pattern. In addition, we identified a gene expression signature that stratified PAs by location (supratentorial versus infratentorial). Lastly, we also identified a gene expression pattern common to PAs and normal mouse astrocytes and neural stem cells from these distinct brain regions as well as a gene expression pattern shared between PAs and another human glial tumor (ependymoma) arising supratentorially compared with those originating in the posterior fossa. These results suggest that glial tumors share an intrinsic, lineage-specific molecular signature that reflects the brain region in which their nonmalignant predecessors originated. [Cancer Res 2007;67(3):890–900]

Introduction

Pilocytic astrocytoma (PA) is the second most common brain tumor occurring in childhood and adolescence, accounting for 15% of all pediatric brain tumors (1). These tumors are glial fibrillary acidic protein–positive neoplasms, which are classified by WHO as grade 1 astrocytomas. Children with the neurofibromatosis type 1 (NF1) tumor predisposition syndrome are prone to the development of PAs. NF1-associated PAs (NF1-PA) tend to occur within the optic pathway and hypothalamus (2), whereas histologically identical sporadic PAs most commonly arise in the cerebellum. Optic pathway PAs in children with NF1 often behave in a clinically indolent fashion, whereas sporadic examples are more likely to progress and require treatment. Moreover, some PAs harbor atypical pathologic features, exhibit more aggressive clinical behavior, and recur after treatment.

Compared with other pediatric brain tumors, little is known about the genetic changes associated with PA formation and progression. Whereas PAs arising in patients with NF1 inactivate the *NF1* gene, histologically identical sporadic PAs do not harbor *NF1* gene mutations or loss of *NF1* protein (neurofibromin) expression (3, 4). Studies aimed at identifying genetic changes in sporadic PA have reported a variety of genomic abnormalities, including loss of allelic heterozygosity on chromosome 17 (5–7), chromosome 7 and 8 copy gains (8–10), and case reports of *PTEN* and oncogenic *KRAS* gene mutations (11, 12). However, none of these genetic changes are consistently found in PAs, suggesting that other molecular changes are involved in PA pathogenesis.

In the absence of specific clinically predictive genetic changes, studies of other solid tumors have successfully used genomic microarray analyses to identify transcriptosome signatures that accurately stratify tumors based on their clinical behavior (13, 14). Accordingly, we have done microarray-based gene expression profiling on the largest published series of PAs to date (n = 41) in an effort to identify patterns of gene expression related to clinically or biologically relevant subgroups. In addition to identifying a genetic signature specifically associated with PA in NF1 patients, we have also identified a genetic signature that distinguishes tumors arising in supratentorial regions from those originating in the posterior fossa. Moreover, a component of this molecular signature is discernible in nonmalignant astrocytes and neural stem cells derived from these brain regions and in another glial tumor type, ependymoma. These data provide the first evidence for molecular heterogeneity among PAs based on brain region.

Materials and Methods

Human specimens. Frozen tumor tissue specimens were obtained from the Siteman Cancer Center Tissue Procurement Core Facility at Washington University (St. Louis, MO), University of Texas M. D. Anderson Cancer Center (Houston, TX), and the Department of Neuropathology, Heinrich-Heine University (Düsseldorf, Germany). Formalin-fixed PA tissue sections were obtained from the M. D. Anderson Cancer Center. Additional paraffin-embedded PA tissue sections, as well as an ependymoma tissue microarray, were generated by the Siteman Cancer Center Tissue Procurement Core Facility. All tissue samples were obtained with informed consent according to established Human Studies Protocols at Washington University and the M. D. Anderson Cancer Center. The use of archival tissue from the Department of Neuropathology in Düsseldorf was approved by the local institutional review board at Heinrich-Heine University. For all frozen tumor samples subjected to microarray analysis, a serial 5-μm section was histologically reviewed to confirm neoplastic cell content by an experienced

Note: Supplementary data for this article are available at Cancer Research Online (http://cancerres.aacrjournals.org/).

Gene Expression Omnibus series accession numbers: GSE5675 (pilocytic astrocytoma data set) and GSE5582 (neocortical and cerebellar astrocyte data set).

Requests for reprints: David H. Gutmann, Department of Neurology, Washington University School of Medicine, Box 8111, 660 South Euclid Avenue, St. Louis, MO 63110. Phone: 314-362-7379; Fax: 314-362-2388; E-mail: gutmannd@wustl.edu.

doi:10.1158/0008-5472.CAN-06-0973

neuropathologist (A.P., K.D.A., or G.R.). Tumors that exhibited significant growth during the course of therapy or within 1 year of initial gross total resection, as well as tumors with high mitotic indices (>1 mitotic figure per 10 high-power fields) or high proliferative indices (MIB labeling index >5), were classified as "aggressive" PAs. No pilomyxoid tumors were included in this series.

RNA isolation from frozen tissues and microarray analysis. Target preparation and microarray hybridization were done by the Siteman Cancer Center Multiplex Gene Analysis Core Facility. Serial sections of 50 μm were homogenized in TRIzol reagent (Invitrogen, Carlsbad, CA) to extract total RNA from PA samples (n = 41). Five micrograms of RNA from each tumor were converted to double-stranded cDNA using a dT-T7 promoter primer. Purified double-stranded cDNA was then used as template to create biotinylated antisense RNA. The labeled antisense RNA target was quantified and fragmented, and 15 μg were used for microarray hybridization. The complete target preparation procedure was done following the manufacturer's recommendations (Affymetrix, Santa Clara, CA). Labeled targets were hybridized to Affymetrix HG-U133 Plus 2.0 GeneChip microarrays for 16 h and washed following standard protocols. Microarray images were processed using Affymetrix GeneChip Operating Software version 1.4 algorithm. Each array was scaled so that the average probe set hybridization signal intensity value (target intensity) was 1,500. Scaled data for each array were exported to the Siteman Cancer Center Bioinformatics server,[7] merged with the updated gene annotation data for each probe set on the array, and downloaded for further data visualization and analysis. The completely annotated, Minimum Information About a Microarray Experiment–compliant data set can be found at the above noted URL and also at Gene Expression Omnibus.[8] Basic microarray data visualization, data filtering, Student's t test, and hierarchical clustering were done using Spotfire DecisionSite for Functional Genomics (Somerville, MA). The P values obtained from Student's t test were corrected for multiple testing with the Benjamini-Hochberg method (15). The human ependymoma data sets were generously provided by Dr. Richard J. Gilbertson (St. Jude Children's Research Hospital, Memphis, TN).

Unsupervised hierarchical clustering was done on these 41 PA specimens using the following methods: (a) clustering method: unweighted pair group method using arithmetic average (UPGMA), similarity measure: Euclidean distance; (b) clustering method: UPGMA, similarity measure: correlation; (c) clustering method: weighted pair group method using arithmetic average (WPGMA), similarity measure: Euclidean distance; (d) clustering method: WPGMA (weighted average), similarity measure: correlation; and (e) clustering method: Ward's method, similarity measure: half square Euclidean distance.

Probe sets that were absent across all chips and the Affymetrix control probe sets were filtered from the analysis. Selection of probe sets whose signals were significantly different between (a) NF1-PA and sporadic PA and (b) supratentorial tumors versus infratentorial tumors were identified using the significance analysis of microarrays (SAM) algorithm at a false discovery rate of 0% and a q value of 0 (16).

RNA isolation from formalin-fixed, paraffin-embedded tissues. RNA was extracted from 5- to 10-μm consecutive paraffin sections using the High Pure RNA Paraffin Kit (Roche Applied Science, Indianapolis, IN) according to manufacturer's instructions. RNA integrity was judged using RNA 6000 nanochips and the Agilent 2100 Bioanalyzer (Agilent Technologies, Palo Alto, CA). RNA samples were quantified using a NanoDrop ND-1000 spectrophotometer (NanoDrop Technologies, Wilmington, DE).

Primary astrocyte cultures. Murine neocortical and cerebellar astroglial cultures, containing >95% glial fibrillary acidic protein–positive cells (astrocytes), were generated from postnatal day 1 (PN1) wild-type (ICR) pups under identical conditions. The culture conditions were the same as previously described (17).

Neural stem cell cultures. Murine neocortical and cerebellar neural stem cell cultures were generated from PN1 wild-type (ICR) pups and maintained as neurospheres on UltraLow plates (Fisher, St. Louis, MO) as previously described (18).

RNA isolation from mouse tissues and microarray analysis. Total RNA was extracted from neocortical and cerebellar PN1 (n = 5) and PN30 (n = 4) mouse brains as well as passage zero (P0) primary astrocytes (n = 5) and neural stem cells (n = 3) from PN1 murine neocortex and cerebellum using RNeasy Mini Kit (Qiagen, Valencia, CA). RNA samples were quantified and RNA integrity was judged as described above. Target preparation and microarray hybridization were done by the Siteman Cancer Center Multiplex Gene Analysis Core Facility using Affymetrix Mouse Genome 430 2.0 GeneChip microarrays. Basic microarray data visualization and data filtering were done as described above. Fold change was calculated by dividing average neocortical astrocyte values for each probe set by the average cerebellar astrocyte value for each probe set. Statistical significance was determined with Student's t test using Spotfire DecisionSite for Functional Genomics. The P values obtained with Student's t test were corrected for multiple testing by the Benjamini-Hochberg method (15).

Real-time reverse transcription-PCR. The expression of specific genes was examined by real-time reverse transcription-PCR (RT-PCR) using SYBR Green detection chemistry. Five hundred nanograms of total RNA extracted from each of the samples were used to make cDNA. Forty nanograms of cDNA from formalin-fixed, paraffin-embedded tissue RNA and 20 ng of cDNA from the frozen tissue RNA were used as template for PCR amplification with the primers specific for each of the transcripts examined. The primers used for each of the human and mouse genes are listed in Supplementary Table S1.

PCR reactions without cDNA samples were used as negative controls. Each reaction was done in duplicate. SDS system software was used to convert the fluorescent data into cycle threshold (C_T) measurements, and the $\Delta\Delta C_T$ method (19) was used to calculate fold expression, using glyceraldehyde-3-phosphate dehydrogenase as an internal control for human samples and β-actin as an internal control for murine samples.

Immunohistochemistry. Immunohistochemistry was done using anti-PAX3 (1:500; Calbiochem, San Diego, CA), anti-LHX2 (1:100; Chemicon International, Temecula, CA), and anti-GLAST (1:500; ref. 20) polyclonal antibodies, followed by Vectastain ABC development (Vector Laboratories, Burlingame, CA). For GLAST, LHX2, and PAX3 immunohistochemistry, tumors with <5% immunoreactive cells were scored as "negative" and the tumors with >75% immunoreactive cells were scored as "positive." All tumors in our series exhibited either <5% or >75% immunoreactive cells. Fisher's exact test was done to determine the statistical significance of the immunohistochemistry results.

Results

Microarray analysis of PAs. Previous studies from our group (21) and others (22, 23) have examined genome-wide expression patterns in smaller sets of PAs. In the present study, we examined gene expression of >47,000 transcripts and variants representing ~39,000 human genes in PAs arising in the posterior fossa (n = 27), supratentorial regions (hypothalamus, optic nerve, and cerebral hemisphere; n = 10), lateral ventricle (n = 1), and brainstem (n = 3; Fig. 1). Among these samples, five tumors were from patients with NF1 (NF1-PA) and the remaining tumors were from patients without NF1 (non–NF1-PA or sporadic PA).

Unsupervised hierarchical clustering was done on these 41 PA specimens (Fig. 1). Aligned with the dendrogram is the corresponding clinical information (age of patient, gender, location of the tumor, aggressive clinical behavior of the tumor, and NF1 status). At the level of "whole-genome" expression analysis, PAs did not readily segregate based on technical variables, age of patient, gender, tumor aggressiveness, tumor location, or NF1 status.

Identification of genes differentially expressed in NF1-PA and sporadic PA. To determine whether a specific gene expression pattern exists that can distinguish NF1-PAs from sporadic PAs, we

[7] http://bioinformatics.wustl.edu/.
[8] http://www.ncbi.nlm.nih.gov/geo/.

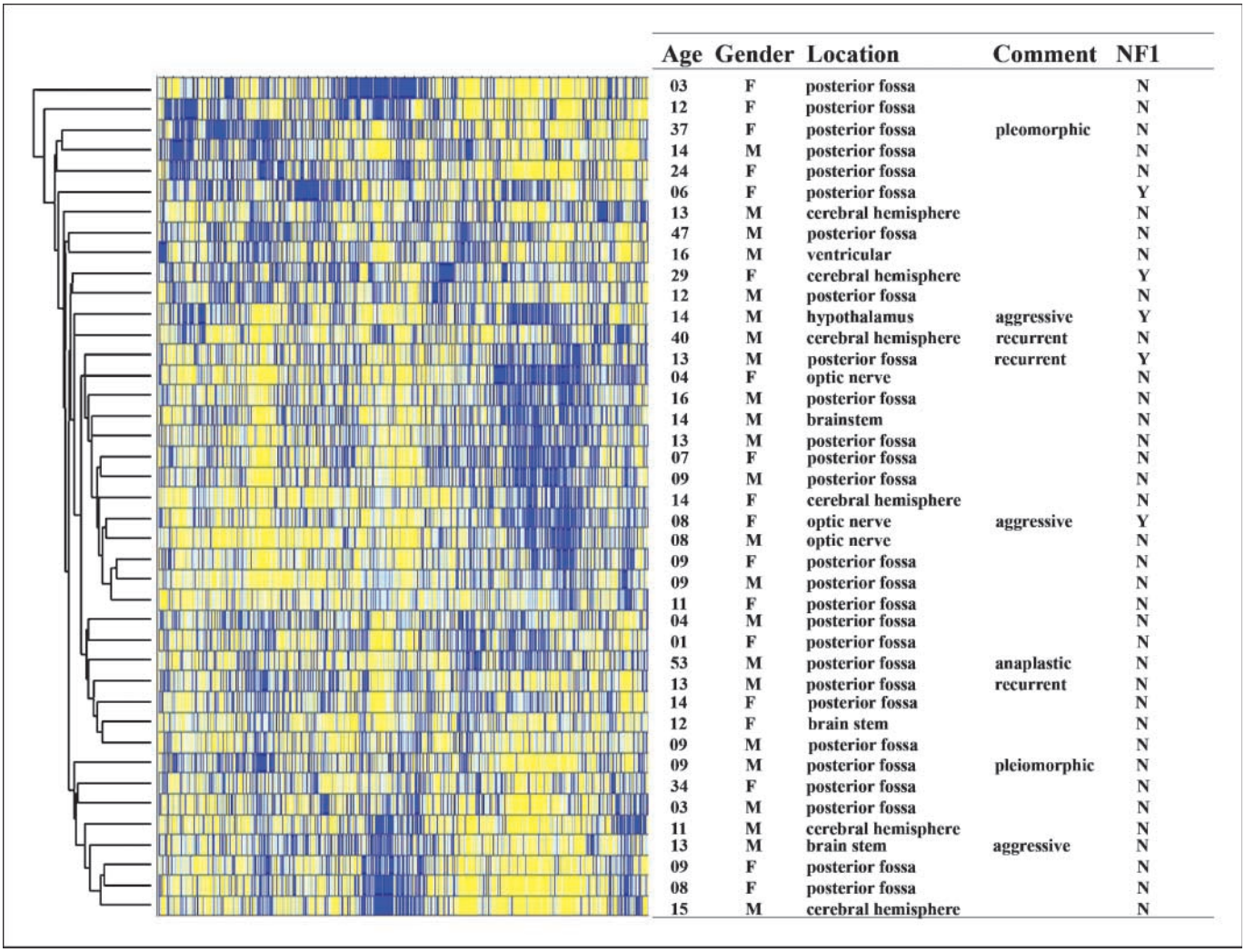

Age	Gender	Location	Comment	NF1
03	F	posterior fossa		N
12	F	posterior fossa		N
37	F	posterior fossa	pleomorphic	N
14	M	posterior fossa		N
24	F	posterior fossa		N
06	F	posterior fossa		Y
13	M	cerebral hemisphere		N
47	M	posterior fossa		N
16	M	ventricular		N
29	F	cerebral hemisphere		Y
12	M	posterior fossa		N
14	M	hypothalamus	aggressive	Y
40	M	cerebral hemisphere	recurrent	N
13	M	posterior fossa	recurrent	Y
04	F	optic nerve		N
16	M	posterior fossa		N
14	M	brainstem		N
13	M	posterior fossa		N
07	F	posterior fossa		N
09	M	posterior fossa		N
14	F	cerebral hemisphere		N
08	F	optic nerve	aggressive	Y
08	M	optic nerve		N
09	F	posterior fossa		N
09	M	posterior fossa		N
11	F	posterior fossa		N
04	M	posterior fossa		N
01	F	posterior fossa		N
53	M	posterior fossa	anaplastic	N
13	M	posterior fossa	recurrent	N
14	F	posterior fossa		N
12	F	brain stem		N
09	M	posterior fossa		N
09	M	posterior fossa	pleiomorphic	N
34	F	posterior fossa		N
03	M	posterior fossa		N
11	M	cerebral hemisphere		N
13	M	brain stem	aggressive	N
09	F	posterior fossa		N
08	F	posterior fossa		N
15	M	cerebral hemisphere		N

Figure 1. Hierarchical cluster analysis of patient PA specimens. Gene expression data were filtered, *z*-score normalized (SD of 1 across all samples for each gene), and subjected to hierarchical cluster analysis as described in the text. The dendrogram on the left displays the relationship of the samples based on their global pattern of gene expression. On the right of the dendrogram is a "heat map" representing gene expression, with each of the 41 samples represented in a row, each probe set represented as a vertical line, and the relative expression of any one gene in any one sample in continuous color scale from low (*yellow*) to high (*dark blue*) expression. Age of patient, gender, tumor location, additional features (comment), and NF1 status (*Y,* NF1-PA; *N,* non–NF1-PA or sporadic PA) are provided for each of the PA samples studied.

used the SAM algorithm (16) to identify genes whose expression differs between NF1-PA and sporadic PA. After data filtering, the analysis was done using 43,527 probe sets. We identified 12 genes, represented by 13 probe sets, which were up-regulated in NF1-PA compared with sporadic PA (Fig. 2*A*). Interestingly, no genes were found whose expression was decreased in NF1-PA relative to sporadic PA. To validate the expression of a subset of these genes, we analyzed the expression of TAK1-like protein (*c21ORF7/TAKL-1*), similar to formin binding protein 2 (similar to *SRGAP2*) and solute carrier family 1 member 3 (*SLC1A3*) transcripts, by quantitative RT-PCR in 5 NF1-PAs and 10 sporadic PAs (Fig. 2*B*). We observed a relatively increased expression in NF1-PAs compared with sporadic PAs for *TAKL-1* ($P = 0.006$, Mann-Whitney rank sum test), similar to *SRGAP2* and *SLC1A3* ($P = 0.017$, Mann-Whitney rank sum test), thus confirming our microarray results. Although there were two cases of sporadic PA that showed higher levels of *TAKL-1* expression consistent with NF1-PAs, these sporadic cases did not exhibit a more indolent behavior compared with the other sporadic PAs. Sporadic PAs with increased *SRGAP2* expression and one NF1-PA with lower *SRGAP2* expression were not clinically different than the other tumors in their corresponding group. Similarly, the one NF1-PA with increased *SLC1A3* expression was not clinically different than the other NF1-PAs.

Using an independent set of tumor RNA from formalin-fixed, paraffin-embedded PA specimens ($n = 10$, sporadic PA; $n = 7$, NF1-PA), we validated the expression of *DCAMKL1, OBFC1, MASS1, EPB41L2*, and *CUGBP2*. In comparison with sporadic PA, the average *DCAMKL1* mRNA levels were increased >2-fold in NF1-PA ($P = 0.035$, Student's t test; Fig. 2*C*) whereas the average *OBFC1* levels were increased >2.5-fold in NF1-PA ($P = 0.007$, Student's t test; Fig. 2*C*). Similarly, average *MASS1* mRNA levels were increased ~2-fold in NF1-PA compared with sporadic PA ($P = 0.038$, Student's t test; Fig. 2*C*). We also observed increased *EPB41L2* (1.6-fold) and *CUGBP2* (1.9-fold) expression in NF1-PA compared with sporadic PA; however, the differences did not reach statistical significance (data not shown).

To compare microarray results with corresponding protein levels, we analyzed SLC1A3 (GLAST) expression by immunohistochemistry. We observed GLAST protein expression in four of nine NF1-PAs compared with two of nine sporadic PAs, similar to the pattern of differential gene transcription identified by microarray analysis; however, these differences did not reach statistical significance (Supplementary Fig. S1). Unfortunately, the lack of antibodies suitable for immunohistochemical analysis precluded validation of the other differentially expressed genes at the protein level.

Identification of genes differentially expressed in supratentorial PA and posterior fossa PA. Recent studies have shown that the brain regions in which another glial cell tumor (ependymoma) develops are associated with unique patterns of gene expression (24). To determine whether a similar genetic signature exists for PAs, we divided our PAs in two subgroups: supratentorial PA (hypothalamus/optic nerve, cerebral hemisphere) and posterior fossa PA. SAM analysis of the 43,294 probe sets after data filtering for these two subgroups of PAs identified 28 genes (represented by 30 probe sets) with increased expression in supratentorial PAs and 8 genes (represented by 11 probe sets) with decreased expression in supratentorial compared with posterior fossa PAs (Table 1). To validate the expression of a subset of these genes, we used RNA extracted from an independent series of 10 supratentorial and 9 posterior fossa formalin-fixed, paraffin-embedded PA specimens. As shown in Fig. 3*A*, the average levels of *LHX2* and *NR2E1* mRNA expression were 2.5-fold ($P = 0.032$, Student's t test) and 2-fold ($P = 0.041$, Student's t test) higher, respectively, in supratentorial PAs compared with posterior fossa PAs. There was also a 2.5-fold increase in the levels of both *MASS1* mRNA ($P = 0.009$, Student's t test) and *RARB* mRNA ($P = 0.026$, Student's t test) expression in supratentorial PA relative to posterior fossa PA (data not shown).

To validate these findings at the protein level, we chose two representative proteins with differential transcript expression, paired box gene 3 (PAX3) and LIM homeobox 2 (LHX2), for which antibodies were available for paraffin immunohistochemistry. Immunohistochemical analysis was done on an independent series of 10 supratentorial and 10 posterior fossa PAs (M.D. Anderson Cancer Center). PAX3 protein expression was detected in 7 (70%) posterior fossa PAs and 1 (10%) supratentorial PA ($P = 0.020$,

A

Unique Probe Identifier	UniGene ID	Unigene Gene Name	Unigene Gene Symbol	SAM score	Fold change (avg. NF1-PA / avg. Sp-PA)
221211_s_at	**Hs.222802**	**Chromosome 21 open reading frame 7**	**C21orf7 (TAK1-like protein)**	**-7.63**	**5.55**
1556202_at	**Hs.523529**	**Similar to Formin binding protein 2**	**-**	**-6.20**	**2.70**
1566624_at	**Hs.481918**	**Solute carrier family 1 (glial high affinity glutamate transporter), member 3**	**SLC1A3**	**-6.10**	**3.03**
240665_at	Hs.309288	CUG triplet repeat, RNA binding protein 2	CUGBP2	-5.84	2.44
1556203_a_at	**Hs.523529**	**Similar to Formin binding protein 2**	**-**	**-5.76**	**2.86**
242903_at	Hs.520414	Interferon gamma receptor 1	IFNGR1	-5.67	2.94
237361_at	**Hs.507755**	**Doublecortin and CaM kinase-like 1**	**DCAMKL1**	**-5.67**	**3.70**
240824_at	**Hs.134491**	**Chromosome 21 open reading frame 53**	**OBFC1**	**-5.57**	**2.08**
1556352_at	Hs.551822	cDNA FLJ30440 fis, clone BRACE2009185	-	-5.48	2.56
234871_at	**Hs.482811**	**Monogenic, audiogenic seizure susceptibility 1 homolog (mouse)**	**MASS1**	**-5.46**	**3.70**
205200_at	Hs.476092	C-type lectin domain family 3, member B	TNA	-5.44	3.12
242652_at	Hs.486470	Erythrocyte membrane protein band 4.1-like 2	EPB41L2	-5.35	2.27
1566825_at	Hs.543540	cDNA FLJ31010 fis, clone HLUNG2000174	-	-5.31	2.78

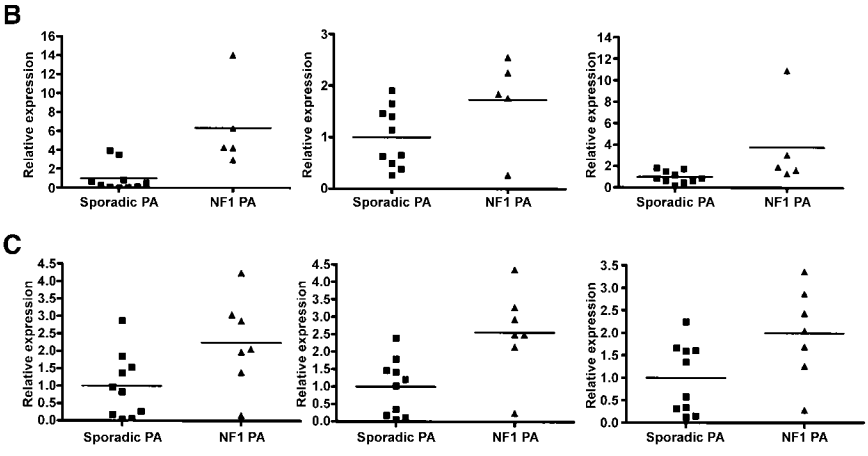

Figure 2. Genes differentially expressed in NF1-PAs and sporadic PAs. *A,* genes differentially expressed in NF1-PAs and sporadic PAs based on SAM at false discovery rate of 0 and a q value of 0. Genes are listed in descending order of significance based on the score assigned by SAM. Genes shown in bold were used for independent validation experiments. *B, TAK1-like* protein (*left*), similar to *SRGAP2* (*middle*) and *SLC1A3* (*right*) mRNA expression, was measured by real-time reverse transcription PCR in 10 sporadic PAs and 5 NF1-PAs. Increased *TAK1-like* protein, similar to *SRGAP2* and *SLC1A3* mRNA expression, was observed in NF1-PAs when compared with sporadic PAs. *C, DCAMKL1* (*left*), *OBFC1* (*middle*), and *MASS1* (*right*) mRNA expression was measured in an independent set of 10 sporadic PAs and 7 NF1-PAs. Increased *DCAMKL1, OBFC1*, and *MASS1* mRNA expression was observed in NF1-PAs compared with sporadic PAs.

Table 1. Genes differentially expressed in supratentorial and posterior fossa PA

Unique probe identifier	UniGene ID	UniGene gene name	UniGene gene symbol	SAM score	Fold change (average ST-PA / average PF-PA)
206140_at	Hs.445265	LIM homeobox 2	*LHX2*	9.23	16.05
211219_s_at	Hs.445265	LIM homeobox 2	*LHX2*	7.80	7.27
241700_at	Hs.458973	Zinc finger homeodomain 4	*ZFHX4*	6.89	3.49
223582_at	Hs.482811	Monogenic, audiogenic seizure susceptibility 1 homologue (mouse)	*MASS1*	6.48	5.41
205080_at	Hs.436538	Retinoic acid receptor, β	*RARB*	6.15	2.49
236277_at	Hs.390616	p21 (CDKN1A)-activated kinase 3	*PAK3*	6.04	2.61
207443_at	Hs.157688	Nuclear receptor subfamily 2, group E, member 1	*NR2E1*	5.81	9.16
206584_at	Hs.69328	Lymphocyte antigen 96	*LY96*	5.58	3.02
218737_at	Hs.144055	Sno, strawberry notch homologue 1 (*Drosophila*)	*SBNO1*	5.54	1.73
222811_at	Hs.72782	Hypothetical protein FLJ11171	*FLJ11171*	5.50	1.63
1561985_at	Hs.335754	Chromosome 14 open reading frame 39	*C14orf39*	5.34	16.33
1562940_at	Hs.568083	cDNA clone IMAGE:5301683		5.33	1.68
228347_at	Hs.558398	Sine oculis homeobox homologue 1 (*Drosophila*)	*SIX1*	5.32	9.53
214830_at	Hs.200738	Solute carrier family 38, member 6	*SLC38A6*	5.30	1.82
226339_at	Hs.21187	TruB pseudouridine (ψ) synthase homologue 1 (*E. coli*)	*TRUB1*	5.28	1.72
204205_at	Hs.474853	Apolipoprotein B mRNA editing enzyme, catalytic polypeptide like 3G	*APOBEC3G*	5.12	2.15
201744_s_at	Hs.406475	Lumican	*LUM*	5.07	5.08
205905_s_at	Hs.549053	MHC class I polypeptide-related sequence A	*MICA*	5.03	1.84
227038_at	Hs.48343	Hypothetical protein MGC26963	*MGC26963*	5.02	2.46
207181_s_at	Hs.9216	Caspase 7, apoptosis-related cysteine peptidase	*CASP7*	4.97	1.64
204523_at	Hs.181552	Zinc finger protein 140 (clone pHZ-39)	*ZNF140*	4.97	1.64
207250_at	Hs.194756	Sine oculis homeobox homologue 6 (*Drosophila*)	*SIX6*	4.96	9.41
227059_at	Hs.444329	Glypican 6	*GPC6*	4.92	2.51
214078_at	Hs.390616	p21 (CDKN1A)-activated kinase 3	*PAK3*	4.90	2.47
206634_at	Hs.503113	Sine oculis homeobox homologue 3 (*Drosophila*)	*SIX3*	4.89	8.28
226117_at	Hs.310640	TRAF-interacting protein with a forkhead-associated domain	*TIFA*	4.81	1.77
202352_s_at	Hs.4295	Proteasome (prosome, macropain) 26S subunit, non-ATPase, 12	*PSMD12*	4.81	1.34
201659_s_at	Hs.372616	ADP-ribosylation factor–like 1	*ARL1*	4.78	1.69
213172_at	Hs.79170	Tetratricopeptide repeat domain 9	*TTC9*	4.74	3.16
214770_at	Hs.446291	Macrophage scavenger receptor 1	*MSR1*	4.74	2.43
231666_at	Hs.42146	Paired box gene 3 (Waardenburg syndrome 1)	*PAX3*	−10.96	0.03
228462_at	Hs.282089	Iroquois homeobox protein 2	*IRX2*	−7.47	0.19
210239_at	Hs.435730	Iroquois homeobox protein 5	*IRX5*	−6.18	0.11
1553485_at	Hs.350729	Hypothetical protein FLJ32447	*FLJ32447*	−5.57	0.24
216059_at	Hs.42146	Paired box gene 3 (Waardenburg syndrome 1)	*PAX3*	−5.50	0.06
212816_s_at	Hs.533013	Cystathionine β-synthase	*CBS*	−5.40	0.43
203185_at	Hs.379970	Ras association (RalGDS/AF-6) domain family 2	*RASSF2*	−5.11	0.47
230463_at	Hs.445503	Synapsin II	*SYN2*	−4.98	0.33
243879_at	Hs.445503	Synapsin II	*SYN2*	−4.75	0.24
212561_at	Hs.501857	RAB6 interacting protein 1	*RAB6IP1*	−4.61	0.66
1553972_a_a	Hs.533013	Cystathionine β-synthase	*CBS*	−4.52	0.45

NOTE: Genes with increased or decreased expression in supratentorial PA are listed in descending order of significance based on the score assigned by SAM.

Fisher's exact test; Fig. 3*B*). Conversely, LHX2 expression was detected in 2 (20%) posterior fossa PAs and 9 (90%) supratentorial PAs ($P = 0.005$, Fisher's exact test; Fig. 3*C*). These results validate the RNA results at the protein level and suggest that PAs arising in specific brain regions have unique molecular signatures.

Because several of these differentially expressed genes encode proteins previously implicated in hindbrain and forebrain development, we sought to determine whether other developmentally regulated genes important in forebrain and hindbrain development were likewise differentially expressed in PAs arising in different brain regions. The genes involved in forebrain (GO ID-GO: 0030900) and hindbrain (GO ID-GO: 0030902) development were obtained from AmiGO.[9] The probe sets that represent these

[9] http://www.godatabase.org/.

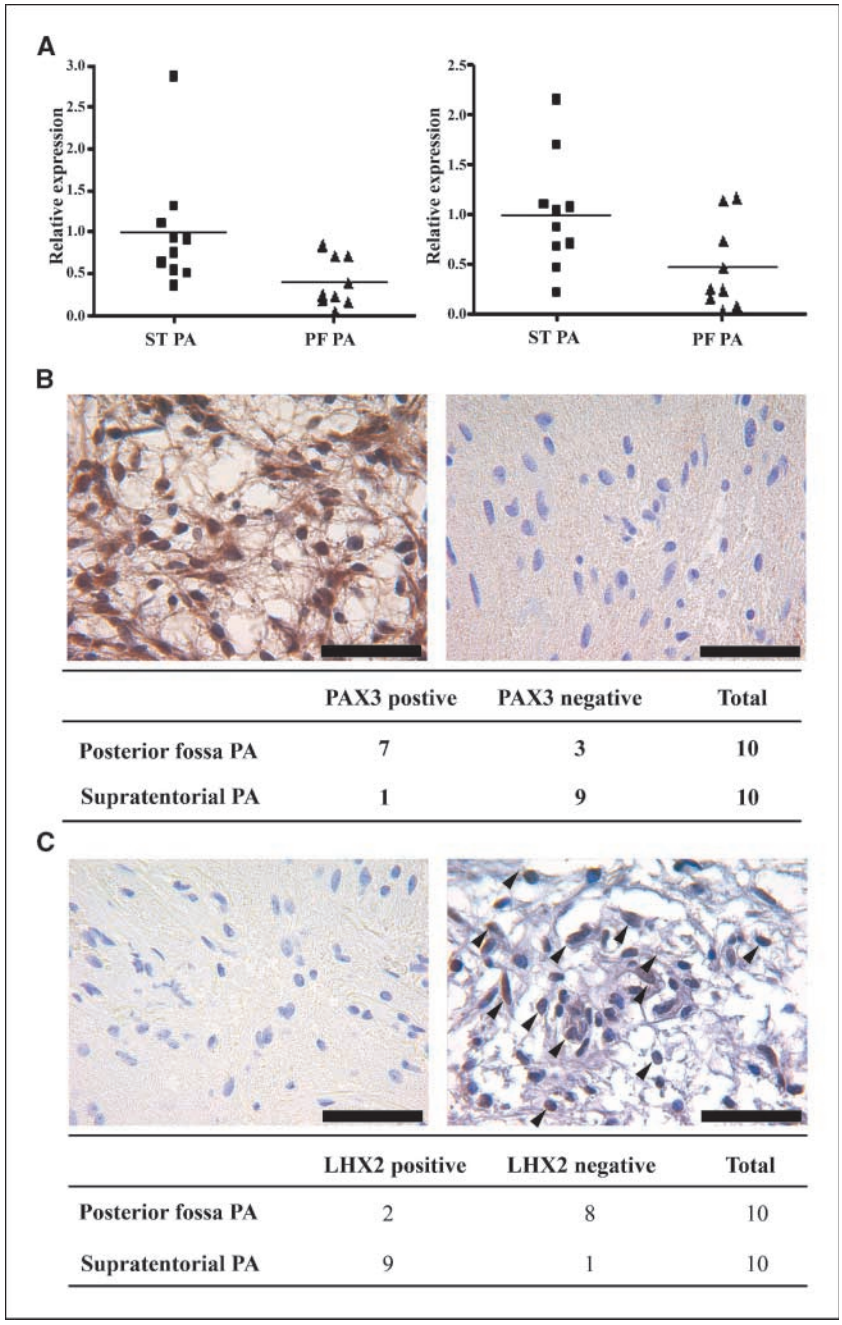

Figure 3. Genes differentially expressed in supratentorial and posterior fossa PAs. *A, LHX2* (*left*) and *NR2E1* (*right*) mRNA expression was measured by real-time reverse transcription PCR in an independent series of formalin-fixed, paraffin-embedded supratentorial (*ST-PA*; $n = 10$) and posterior fossa (*PF-PA*; $n = 9$) PAs. Increased *LHX2* and *NR2E1* mRNA expression was observed in supratentorial PAs compared with posterior fossa PAs. *B,* immunohistochemical analysis of PAX3 protein expression in supratentorial and posterior fossa PAs. PAX3 protein expression is shown for a representative posterior fossa PA (*left*) and a representative supratentorial PA (*right*). A summary of the PAX3 staining results in posterior fossa and supratentorial PAs from an independent series of samples is shown in the table. The proportion of posterior fossa tumors immunoreactive for PAX3 protein expression was statistically different from that observed in supratentorial tumors ($P = 0.020$, Fisher's exact test). *C,* immunohistochemical analysis of LHX2 protein expression in supratentorial and posterior fossa PAs. LHX2 protein expression is shown for a representative posterior fossa PA (*left*) and a representative supratentorial PA (*right*). A summary of the LHX2 staining results in posterior fossa and supratentorial PAs from an independent series of samples is shown in the table. The proportion of supratentorial tumors positive for LHX2 protein expression was statistically different from that observed in posterior fossa tumors ($P = 0.005$, Fisher's exact test). *Bar*, 50 μm. *Arrows,* nuclear LHX2 immunoreactivity.

genes in our microarray data sets were obtained using the Function Express algorithm[10] (Siteman Cancer Center Bioinformatics Core). Hierarchical clustering was done using this set of developmental marker transcripts to determine whether genes involved in cortical (forebrain) versus cerebellar (hindbrain) development would suffice to distinguish supratentorial from posterior fossa PA. In fact, this class of developmentally regulated transcripts themselves could not distinguish PAs by site of origin (Supplementary Fig. S2*A*).

Similarly, to identify genes that exhibit either differential gene expression in normal human brain (neocortex) versus cerebellum, we obtained expression data for all normal human tissues available as Human U133A GeneChip microarray data sets (gcRMA-condensed) from the GeneAtlas project at the Genomics Institute of the Novartis Research Foundation.[11] The median expression value for each available probe set over all the tissues was calculated. The probe sets that had either 10-fold higher or 10-fold lower values in whole brain (cortex) or cerebellum compared with the calculated median were selected for further analysis. Hierarchical clustering was done again on our PA tumor data set using this set of transcripts to determine whether genes that are either up-regulated or down-regulated in cortex (forebrain) versus

[10] http://bioinformatics.wustl.edu/webTools/FunctionExpressClient.do.

[11] http://wombat.gnf.org/index.html.

cerebellum (hindbrain) would distinguish supratentorial from posterior fossa PAs. The results show that this class of transcripts themselves could also not distinguish PAs by site of origin (Supplementary Fig. S2*B*). These negative results strengthen the contention that the signature we have identified between supratentorial versus posterior fossa PAs is unique and specific to PAs arising in these distinct brain locations and does not merely recapitulate brain region developmental gene expression patterns.

Expression in normal murine tissues, astrocytes, and neural stem cells. To determine whether the region-specific gene expression patterns in PAs reflected regional differences in glial-specific gene expression, we examined gene expression in murine neocortical and cerebellar primary astrocyte cultures by Affymetrix GeneChip microarray analysis (n = 3 individual cultures per region). After data filtering, 30,505 probe sets were obtained for analysis. We used the set of 36 genes (represented by 41 probe sets) identified as differentially expressed in supratentorial versus posterior fossa human PAs to query this new data set for similar patterns of gene expression. Of these 36 genes, we identified 6 genes that are differentially expressed in both the supratentorial versus posterior fossa human PAs and the neocortical versus cerebellar mouse astrocytes (Fig. 4*A*). Using real-time RT-PCR, we examined the expression of five of these genes in mouse brain at PN1 and PN30. We chose two genes with increased expression (*LHX2* and *NR2E1*) and three genes with decreased expression (*IRX2, PAX3*, and *IRX5*) in supratentorial versus posterior fossa PAs. As shown in Fig. 4*B*, *LHX2* and *NR2E1* mRNA levels were 9- and 10-fold higher in PN1 neocortex compared with PN1 cerebellum (P < 0.001, Student's t test). At PN30, expression of both transcripts remained elevated (*LHX2,* P < 0.001, Student's t test; *NR2E1,* P = 0.044, Student's t test) in the neocortex compared with the cerebellum (Fig. 4*B, top*). Conversely, *IRX2* and *PAX3* mRNA levels were increased 7- and 9-fold in PN1 cerebellum compared with PN1 neocortex (Fig. 4*B, top*). After the early postnatal period (PN30), the level of *IRX2* mRNA was 3-fold higher and the level of *PAX3* mRNA was 21-fold higher in the cerebellum than in the neocortex (Fig. 4*B, top*). *IRX5* mRNA levels also showed a similar trend of increased expression in the cerebellum compared with both the neocortex at PN1 (10-fold; P < 0.001, Student's t test; data not shown) and at PN30 (5-fold; P = 0.005, Student's t test; data not shown).

To determine whether this differential gene expression pattern was retained in primary glial fibrillary acidic protein–positive cells (astrocytes) isolated from these regions, we analyzed *LHX2, NR2E1, IRX2, PAX3*, and *IRX5* mRNA expression in neocortical

A

Unique Probe Identifier (MG-430 2.0)	UniGene ID	Unigene Gene Name	Unigene Gene Symbol	Fold Change Astrocyte (average CTX/ average CB)	Corrected p-value (astrocytes)	Unique Probe Identifier (HG-U133 Plus2.0)	Fold change PA (average ST PA/ average PF PA)	Corrected p-value (PAs)
1427523_at	Mm.370208	Sine oculis homeobox homolog 3 (Drosophila)	Six3	6.17	0.033	206634_at	8.28	2.01E-02
1418317_at	Mm.142856	LIM homeobox 2	Lhx2	52.53	0.014	206140_at 211219_s_at	16.05 7.27	1.31E-06 3.55E-05
1434921_at 1457289_at	Mm.287100	Nuclear receptor subfamily 2, group E, member 1	Nr2e1	243.1 29.99	0.011 0.045	207443_at	9.16	3.47E-03
1426298_at	Mm.28888	Iroquois homeobox protein 2 (Drosophila)	Irx2	0.076	0.045	228462_at	0.19	8.11E-05
1420389_at	Mm.1371	Paired box gene 3	Pax3	0.017	0.029	216059_at 231666_at	0.06 0.03	3.60E-03 2.15E-08
1421072_at	Mm.101153	Iroquois homeobox protein 5 (Drosophila)	Irx5	0.138	0.039	210239_at	0.11	0.002

B

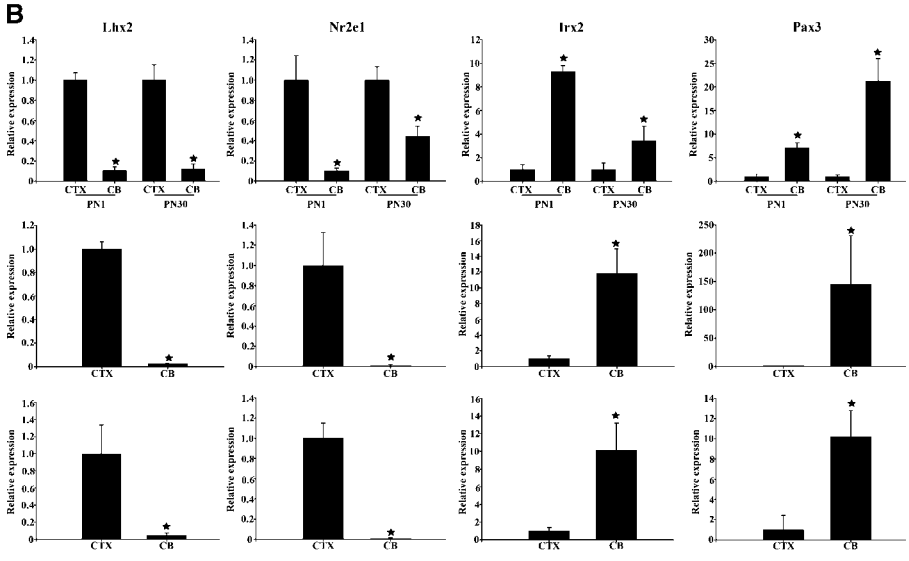

Figure 4. Murine brain, astrocyte, and neural stem cell mRNA expression of genes differentially expressed in PAs. *A,* analysis of the differentially expressed PA genes (Table 1) in mouse brain and astrocytes. Genes with increased mRNA expression in supratentorial or posterior fossa PAs and neocortical (*CTX*) or cerebellar (*CB*) astrocytes are presented. Statistically significant differences (P values by Benjamini-Hochberg–corrected Student's t test) are included for both the original PA microarray data and the astrocyte microarray data. *B, LHX2, NR2E1, IRX2*, and *PAX3* mRNA expression was examined in PN1 and PN30 mouse neocortex and cerebellum (*upper*), in primary PN1 neocortical and cerebellar astrocytes (*middle*), as well as in PN1 neocortical and cerebellar neural stem cells (*NSC; lower*). In each analysis, mRNA levels were normalized to neocortex, neocortical astrocytes, or neocortical neural stem cells (relative value = 1.0). *, P < 0.05.

and cerebellar astrocytes generated from PN1 mice. In these experiments, *LHX2* mRNA expression was increased 40-fold in neocortical compared with cerebellar astrocytes ($P = 0.008$, Mann-Whitney rank sum test), whereas *NR2E1* expression was increased 108-fold between these two astrocyte populations ($P = 0.008$, Mann-Whitney rank sum test; Fig. 4*B, middle*). Conversely, *IRX2* mRNA expression was increased 12-fold in cerebellar compared with neocortical astrocytes ($P = 0.008$, Mann-Whitney rank sum test), whereas *PAX3* expression was increased 145-fold ($P = 0.008$, Mann-Whitney rank sum test; Fig. 4*B, middle*). *IRX5* mRNA levels were increased 10-fold in cerebellar compared with neocortical astrocytes ($P < 0.001$, Student's t test; data not shown).

To provide additional support for a brain region–specific gene expression pattern, we next examined normal neural stem cells, which give rise to astrocytes *in vitro* and *in vivo*, to determine whether the differential gene expression pattern presented in Fig. 4*A* was retained in neural stem cells isolated from PN1 mouse neocortex and cerebellum. In these experiments, the *LHX2* mRNA expression was increased 20-fold in neocortical compared with cerebellar neural stem cells ($P = 0.008$, Student's t test), whereas *NR2E1* expression was increased 96-fold between these two neural stem cell populations ($P < 0.001$, Student's t test; Fig. 4*B, bottom*). Conversely, *IRX2* mRNA expression was increased 10-fold in cerebellar compared with neocortical neural stem cells ($P = 0.007$, Student's t test), whereas *PAX3* expression was increased 10-fold ($P = 0.006$, Student's t test; Fig. 4*B, bottom*). *IRX5* mRNA levels were increased 7.5-fold in cerebellar compared with neocortical neural stem cells ($P = 0.005$, Student's t test; data not shown). These results show that the differential gene expression pattern presented in Fig. 4*A* is retained in neural stem cells, astrocytes, and PAs that arise in these distinct brain regions.

Identification of genes differentially expressed in supratentorial versus posterior fossa ependymomas. Because astrocytomas and ependymomas are both glial cell tumors, we next sought to determine whether the differential pattern of gene expression was shared by these two glial tumors. The ependymoma microarray gene expression data sets were generously provided by Dr. Richard J. Gilbertson (24), and the fold change in expression between supratentorial and posterior fossa ependymomas was calculated for each probe set with statistical significance set at $P < 0.05$ (Benjamini-Hochberg–corrected Student's t test). The probe sets previously identified to be differentially expressed in supratentorial versus posterior fossa PAs (Table 1) were used to query the ependymoma microarray data set. We found seven genes that were differentially expressed in supratentorial versus posterior fossa ependymomas (Fig. 5*A*). Six of these transcripts were increased (*LHX2, NR2E1, SIX3, TTC9, CASP7*, and *ZNF140*) whereas one was decreased (*RASSF2*) in supratentorial ependymomas relative to posterior fossa ependymomas. *PAX3* was previously reported to be increased in posterior fossa ependymomas relative to ependymomas arising supratentorially or in the spinal cord (24).

We next sought to determine whether the differential expression pattern of PAX3 and LHX2 mRNA observed in PAs, ependymoma, primary astrocyte cultures, and neural stem cells could be validated at the protein level. Immunohistochemistry was done to determine the expression of PAX3 protein in 30 ependymomas arising in the posterior fossa and 7 supratentorial ependymomas. Consistent with our observations in PAs, increased PAX3 protein expression was detected in 28 (93%) posterior fossa ependymomas, but in none of the supratentorial ependymomas ($P < 0.001$, Fisher's exact test; Fig. 5*B*). LHX2 protein expression was examined in 31 posterior fossa ependymomas and 8 supratentorial ependymomas. As observed in the PAs, increased LHX2 protein expression was found in 3 (9.7%) of the posterior fossa ependymomas and in 8 (100%) of the supratentorial ependymomas ($P < 0.001$, Fisher's exact test; Fig. 5*C*).

Collectively, these results suggest that despite the considerable biological heterogeneity of ependymomas and PAs, these tumors share an intrinsic, lineage-specific molecular signature that reflects the brain region in which their nonmalignant predecessors originated.

Discussion

PAs are low-grade gliomas that lack the typical molecular alterations associated with diffuse high-grade astrocytomas. In an effort to identify genetic signatures that might correlate with clinically or biologically relevant subgroups of PA, we used microarray-based gene expression profiling on a large set of 41 PAs.

In this study, we were unable to identify genes that could distinguish tumors with statistical certainty based on clinical behavior (recurrence or histologically aggressive features), age of patient, or patient gender. A recent study by Wong et al. (23) examined a smaller series of 25 PAs. Using a similar approach to the one described in this study, they subdivided tumors into two groups and identified genes associated with tumor persistence or tumor recurrence after initial surgical resection. When we examined the expression of these differentially expressed genes in our own set of PAs, we found that these genes did not discriminate clinically aggressive PAs from more indolent cases. Moreover, we specifically examined the expression of one of these transcripts, myelin basic protein, at the RNA and protein levels, and found no differential expression in clinically aggressive PA (RNA) or in NF1-PA versus sporadic PA (RNA and protein).[12] These findings further underscore the current lack of a reliable genetic signature to predict the clinical behavior of these tumors.

The observation that NF1-PAs tend to be clinically less aggressive, particularly when located in the optic pathway (2, 25), coupled with the finding that *NF1* inactivation is only found in NF1-PAs, suggests that NF1-PAs have a unique set of genetic changes in addition to *NF1* loss. Using SAM analysis to identify transcripts differentially expressed in NF1-PA compared with sporadic PA, we found a limited number of NF1-PA-specific transcripts, all of which were up-regulated relative to sporadic PA. A few of these differentially expressed transcripts have known functions (CUGBP2 and SLC1A3 or GLAST; refs. 26–29); however, for most of the transcripts, no functional studies have been done [TAKL-1/c21ORF7, similar to SRGAP2, chromosome 21 open reading frame 53 (OBFC1), cDNA FLJ340440, and cDNA FLJ31010]. It should also be noted that none of these genes were differentially expressed in *Nf1*-deficient murine astrocytes or neural stem cells compared with wild-type controls,[12] suggesting that these differentially expressed transcripts reflect a molecular signature unique to NF1-PAs and do not directly result from *NF1* loss in glial cells.

Perhaps the most intriguing finding of the present study was the identification of a differential gene expression pattern associated with PAs arising in supratentorial versus posterior fossa (infratentorial) locations. A number of these differentially expressed

[12] M.K. Sharma and D.H. Gutmann, unpublished results.

A

Unique Probe Identifier	UniGene ID	Unigene Gene Name	Unigene Gene Symbol	Fold change PA (average ST/ average PF)	Corrected *p*-value (PA)	Fold Change Ependymoma (average ST/ average PF)	Corrected *p*-value (Ependymoma)
206140_at	Hs.445265	LIM homeobox 2	LHX2	16.05	1.31E-06	146.7	1.13E-04
211219_s_at				7.27	3.55E-05	15.83	1.54E-11
207443_at	Hs.157688	Nuclear receptor subfamily 2, group E, member 1	NR2E1	9.16	3.47E-03	47.39	2.23E-03
206634_at	Hs.503113	Sine oculis homeobox homolog 3 (Drosophila)	SIX3	8.28	2.01E-02	7.33	1.38E-02
213172_at	Hs.79170	Tetratricopeptide repeat domain 9	TTC9	3.16	2.93E-02	2.05	4.57E-02
207181_s_at	Hs.9216	Caspase 7, apoptosis-related cysteine peptidase	CASP7	1.64	1.85E-02	2.16	9.02E-03
204523_at	Hs.181552	Zinc finger protein 140 (clone pHZ-39)	ZNF140	1.64	1.95E-02	1.61	4.23E-02
216059_at	Hs.42146	Paired box gene 3 (Waardenburg syndrome 1)	PAX3	0.06	3.60E-03	0.12	7.48E-02
203185_at	Hs.379970	Ras association (RalGDS/AF-6) domain family 2	RASSF2	0.47	1.85E-02	0.30	4.48E-02

B

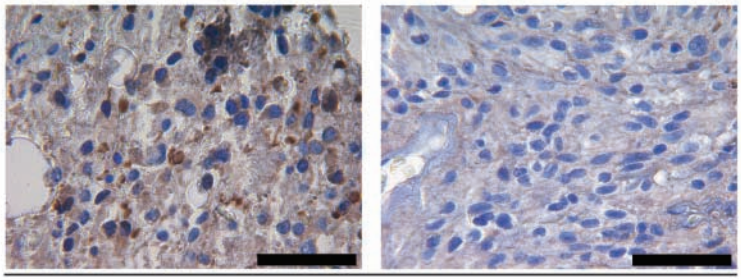

	PAX3 positive	PAX3 negative	Total
Posterior fossa	28	2	30
Supratentorial	0	7	7

C

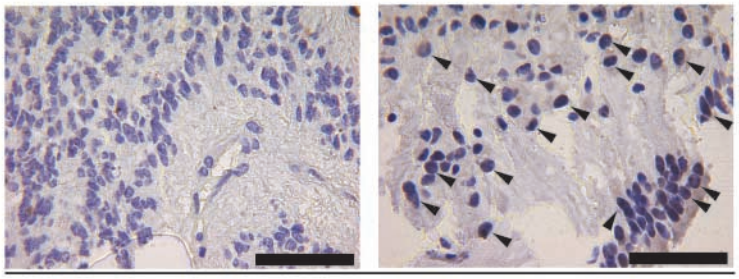

	LHX2 positive	LHX2 negative	Total
Posterior fossa	3	28	31
Supratentorial	8	0	8

Figure 5. Ependymoma mRNA expression of the genes differentially expressed in PA. *A,* analysis of the differentially expressed PA genes (Table 1) in supratentorial and posterior fossa ependymomas. Genes with increased mRNA expression in supratentorial (ST-PA) or posterior fossa (PF-PA) PAs and supratentorial (ST) or posterior fossa (PF) ependymomas are presented. Statistically significant differences (*P* values by Benjamini-Hochberg–corrected Student's *t* test) are included for both the original PA microarray data and the ependymoma microarray data. *B,* immunohistochemical analysis of PAX3 protein expression in supratentorial and posterior fossa ependymomas. PAX3 protein expression is shown for a representative posterior fossa ependymoma (*left*) and a representative supratentorial ependymoma (*right*). The immunohistochemistry results for PAX3 protein expression in posterior fossa and supratentorial ependymoma samples are shown in the table. The proportion of posterior fossa tumors with tumoral PAX3 immunoreactivity was statistically different from that observed in supratentorial tumors ($P < 0.001$, Fisher's exact test). *C,* immunohistochemical analysis of LHX2 protein expression in supratentorial and posterior fossa ependymomas. LHX2 protein expression is shown for a representative posterior fossa ependymoma (*left*) and a representative supratentorial ependymoma (*right*; *arrowheads*). The immunohistochemistry results for LHX2 protein expression in posterior fossa and supratentorial ependymoma samples are shown in the table. The proportion of supratentorial tumors with LHX2 immunoreactivity was statistically different from that observed in posterior fossa tumors ($P < 0.001$, Fisher's exact test). *Bar*, 50 μm.

transcripts have previously been implicated in forebrain (LHX2, NR2E1, and SIX3) and hindbrain (PAX3, IRX2, and IRX5) development. For example, we found increased *LHX2* RNA and protein expression in supratentorial PA. LHX2 is expressed in the developing forebrain during embryogenesis and its inactivation in $LHX2^{-/-}$ mice results in reduced size of the cerebral cortex and impaired cortical hem formation (30–32). NR2E1 (tailless; TLX) is expressed in the developing forebrain (33) and loss of NR2E expression results in an overall reduced thickness of superficial cortical layers (34). Similarly, Six3 expression is restricted to the anterior neural plate and its function is essential for normal vertebrate forebrain development (35, 36). Conversely, we found that PAX3 and IRX2 expression was increased in posterior fossa PAs. Both PAX3 and IRX2 are expressed in the developing hindbrain (37–39). In addition, PAX3 is one of the development signals critical for proper hindbrain differentiation (40), and PAX3-deficient mice (Splotch mutant mice) exhibit neural tube closure defects and abnormal brain development (41). IRX2 and IRX5 are members of the Iroquois class of homeobox genes, and IRX2 is involved in vertebrate cerebellar development (39).

The identification of transcripts that reflect the developmental origin of tumors from specific brain regions raised several questions. First, are other genes implicated in hindbrain and forebrain development also differentially expressed in supratentorial versus infratentorial PA? We analyzed the expression of genes known to be associated with hindbrain and forebrain development using two different methods and found that these other genes were not differentially expressed between PAs originating at different sites. This finding suggests that this genetic signature (Fig. 4*A*) is not merely a reflection of normal brain region–specific development but represents a unique set of brain region–specific genes relevant to glioma.

Second, we asked whether this differential gene expression pattern simply reflects tumor contamination by native cellular elements found in those specific brain regions. Whereas these brain region–specific genetic profiles were retained in the postnatal mouse brain (forebrain versus cerebellum), we also found that this genetic signature was present in primary glial fibrillary acidic protein–positive cells (astrocytes) and neural stem cells from forebrain versus cerebellum. These results suggest that this molecular profile is an intrinsic property of cells arising in these specific brain regions. The detection of a genetic signature specific to cerebellar versus neocortical astrocytes and neural stem cells suggests that morphologically indistinguishable glia and stem cells from different brain regions are unique. In this regard, numerous studies have shown that cerebellar and neocortical astrocytes have different biological and electrophysiologic properties (42–45). For example, neocortical astrocytes exhibit increased ATP/ADP hydrolysis (46), as well as increased serotonin and glutamate uptake (47), relative to astrocytes from the cerebellum. One report showed that neural precursor cells from different human embryonic brain regions exhibit different growth properties (48). In this study, precursor cells from the forebrain grew significantly faster than those from the hindbrain. Whereas these findings suggest that populations of astrocytes and neural stem cells from different brain regions have distinct biological properties, additional studies will be required to define the effect of these physiologic properties on the clinical behavior of tumors from these brain regions.

Finally, we sought to determine whether a common site-specific gene expression pattern was shared between PAs and another glial tumor type (ependymoma). In a recent study of ependymoma, Taylor et al. (24) found brain region–specific patterns of gene expression. Using the original microarray data generated by Taylor and colleagues, we found a differential gene expression pattern shared between ependymomas and PAs arising supratentorially compared with those arising in the posterior fossa. In this regard, *LHX2, NR2E1, SIX3, TTC9, CASP7*, and *ZNF140* expression was increased in both supratentorial PA and supratentorial ependymoma, whereas *PAX3* and *RASSF2* expression was increased in both posterior fossa PA and posterior fossa ependymoma. These common findings further support the notion that a brain region–specific gene expression pattern exists for glial cell tumors.

The identification of a brain region–specific gene expression pattern argues that glia and neural stem cells from different brain regions may be distinct and possess unique biological properties relevant to tumorigenesis. Moreover, a shared gene expression pattern between astrocytoma and ependymoma also suggests a common cell of origin for these histologically different tumor types. Future mechanistic studies aimed at defining the precise role of each of these differentially expressed genes may lead to an improved understanding of the molecular and cellular pathogenesis of these common nervous system tumors and potentially result in the development of targeted therapies.

Acknowledgments

Received 3/14/2006; revised 10/5/2006; accepted 11/21/2006.

Grant support: Schnuck Markets, Inc. (D.H. Gutmann), Hyundai Motors (D.B. Mansur), and National Cancer Institute Cancer Center Support grant P30 CA91842 to the Siteman Cancer Center.

The costs of publication of this article were defrayed in part by the payment of page charges. This article must therefore be hereby marked *advertisement* in accordance with 18 U.S.C. Section 1734 solely to indicate this fact.

We thank Sunita B. Koul for technical help during this study and Dr. Veena Rajaram for generating the ependymoma tissue microarray; the Alvin J. Siteman Cancer Center at Washington University School of Medicine and Barnes-Jewish Hospital in St. Louis, MO, for the use of the Tissue Procurement Core; and Dr. Richard J. Gilbertson for generously providing the ependymoma microarray data sets.

References

1. Kleihues P, Sobin LH. World Health Organization classification of tumors. Cancer 2000;88:2887.
2. Listernick R, Darling C, Greenwald M, Strauss L, Charrow J. Optic pathway tumors in children: the effect of neurofibromatosis type 1 on clinical manifestations and natural history. J Pediatr 1995;127:718–22.
3. Kluwe L, Hagel C, Tatagiba M, et al. Loss of NF1 alleles distinguish sporadic from NF1-associated pilocytic astrocytomas. J Neuropathol Exp Neurol 2001;60:917–20.
4. Wimmer K, Eckart M, Meyer-Puttlitz B, Fonatsch C, Pietsch T. Mutational and expression analysis of the NF1 gene argues against a role as tumor suppressor in sporadic pilocytic astrocytomas. J Neuropathol Exp Neurol 2002;61:896–902.
5. von Deimling A, Louis DN, Menon AG, et al. Deletions on the long arm of chromosome 17 in pilocytic astrocytoma. Acta Neuropathol (Berl) 1993;86:81–5.
6. Phelan CM, Liu L, Ruttledge MH, et al. Chromosome 17 abnormalities and lack of TP53 mutations in paediatric central nervous system tumours. Hum Genet 1995;96:684–90.
7. Willert JR, Daneshvar L, Sheffield VC, Cogen PH. Deletion of chromosome arm 17p DNA sequences in pediatric high-grade and juvenile pilocytic astrocytomas. Genes Chromosomes Cancer 1995;12:165–72.
8. White FV, Anthony DC, Yunis EJ, et al. Nonrandom chromosomal gains in pilocytic astrocytomas of childhood. Hum Pathol 1995;26:979–86.
9. Zattara-Cannoni H, Gambarelli D, Lena G, et al. Are juvenile pilocytic astrocytomas benign tumors? A cytogenetic study in 24 cases. Cancer Genet Cytogenet 1998;104:157–60.
10. Sanoudou D, Tingby O, Ferguson-Smith MA, Collins VP, Coleman N. Analysis of pilocytic astrocytoma by comparative genomic hybridization. Br J Cancer 2000;82:1218–22.
11. Duerr EM, Rollbrocker B, Hayashi Y, et al. PTEN mutations in gliomas and glioneuronal tumors. Oncogene 1998;16:2259–64.
12. Sharma MK, Zehnbauer BA, Watson MA, Gutmann DH. RAS pathway activation and an oncogenic RAS mutation in sporadic pilocytic astrocytoma. Neurology 2005;65:1335–6.
13. Ohira M, Oba S, Nakamura Y, et al. Expression profiling using a tumor-specific cDNA microarray predicts the prognosis of intermediate risk neuroblastomas. Cancer Cell 2005;7:337–50.
14. Sotiriou C, Wirapati P, Loi S, et al. Gene expression profiling in breast cancer: understanding the molecular basis of histologic grade to improve prognosis. J Natl Cancer Inst 2006;98:262–72.
15. Benjamini Y, Hochberg Y. Controlling the false discovery rate: a practical and powerful approach to multiple testing. J Roy Stat Soc, Ser B 1995;57:289–300.
16. Tusher VG, Tibshirani R, Chu G. Significance analysis of microarrays applied to the ionizing radiation response. Proc Natl Acad Sci U S A 2001;98:5116–21.
17. Dasgupta B, Yi Y, Chen DY, Weber JD, Gutmann DH. Proteomic analysis reveals hyperactivation of the mammalian target of rapamycin pathway in neurofibromatosis 1-associated human and mouse brain tumors. Cancer Res 2005;65:2755–60.
18. Dasgupta B, Gutmann DH. Neurofibromin regulates neural stem cell proliferation, survival, and astroglial differentiation *in vitro* and *in vivo*. J Neurosci 2005;25:5584–94.
19. Livak KJ, Schmittgen TD. Analysis of relative gene expression data using real-time quantitative PCR and the $2^{-\Delta\Delta C_T}$ method. Methods 2001;25:402–8.
20. Shibata T, Yamada K, Watanabe M, et al. Glutamate transporter GLAST is expressed in the radial glia-astrocyte lineage of developing mouse spinal cord. J Neurosci 1997;17:9212–9.
21. Gutmann DH, Hedrick NM, Li J, et al. Comparative gene expression profile analysis of neurofibromatosis 1-associated and sporadic pilocytic astrocytomas. Cancer Res 2002;62:2085–91.
22. Rickman DS, Bobek MP, Misek DE, et al. Distinctive molecular profiles of high-grade and low-grade gliomas

based on oligonucleotide microarray analysis. Cancer Res 2001;61:6885–91.
23. Wong KK, Chang YM, Tsang YT, et al. Expression analysis of juvenile pilocytic astrocytomas by oligonucleotide microarray reveals two potential subgroups. Cancer Res 2005;65:76–84.
24. Taylor MD, Poppleton H, Fuller C, et al. Radial glia cells are candidate stem cells of ependymoma. Cancer Cell 2005;8:323–35.
25. Chateil JF, Soussotte C, Pedespan JM, et al. MRI and clinical differences between optic pathway tumours in children with and without neurofibromatosis. Br J Radiol 2001;74:24–31.
26. Barreau C, Paillard L, Mereau A, Osborne HB. Mammalian CELF/Bruno-like RNA-binding proteins: molecular characteristics and biological functions. Biochimie 2005;88:515–25.
27. Timchenko NA, Cai ZJ, Welm AL, et al. RNA CUG repeats sequester CUGBP1 and alter protein levels and activity of CUGBP1. J Biol Chem 2001;276:7820–6.
28. Sundholm-Peters NL, Yang HK, Goings GE, Walker AS, Szele FG. Radial glia-like cells at the base of the lateral ventricles in adult mice. J Neurocytol 2004;33:153–64.
29. Hartfuss E, Galli R, Heins N, Gotz M. Characterization of CNS precursor subtypes and radial glia. Dev Biol 2001;229:15–30.
30. Ando H, Kobayashi M, Tsubokawa T, et al. Lhx2 mediates the activity of Six3 in zebrafish forebrain growth. Dev Biol 2005;287:456–68.
31. Bulchand S, Grove EA, Porter FD, Tole S. LIM-homeodomain gene Lhx2 regulates the formation of the cortical hem. Mech Dev 2001;100:165–75.
32. Porter FD, Drago J, Xu Y, et al. Lhx2, a LIM homeobox gene, is required for eye, forebrain, and definitive erythrocyte development. Development 1997;124:2935–44.
33. Monaghan AP, Grau E, Bock D, Schutz G. The mouse homolog of the orphan nuclear receptor tailless is expressed in the developing forebrain. Development 1995;121:839–53.
34. Land PW, Monaghan AP. Abnormal development of zinc-containing cortical circuits in the absence of the transcription factor Tailless. Brain Res Dev Brain Res 2005;158:97–101.
35. Oliver G, Mailhos A, Wehr R, et al. Six3, a murine homologue of the sine oculis gene, demarcates the most anterior border of the developing neural plate and is expressed during eye development. Development 1995;121:4045–55.
36. Lagutin OV, Zhu CC, Kobayashi D, et al. Six3 repression of Wnt signaling in the anterior neuroectoderm is essential for vertebrate forebrain development. Genes Dev 2003;17:368–79.
37. Goulding MD, Chalepakis G, Deutsch U, Erselius JR, Gruss P. Pax-3, a novel murine DNA binding protein expressed during early neurogenesis. EMBO J 1991;10:1135–47.
38. Terzic J, Saraga-Babic M. Expression pattern of PAX3 and PAX6 genes during human embryogenesis. Int J Dev Biol 1999;43:501–8.
39. Matsumoto K, Nishihara S, Kamimura M, et al. The prepattern transcription factor Irx2, a target of the FGF8/MAP kinase cascade, is involved in cerebellum formation. Nat Neurosci 2004;7:605–12.
40. Matsunaga E, Araki I, Nakamura H. Role of Pax3/7 in the tectum regionalization. Development 2001;128:4069–77.
41. Lakkis MM, Golden JA, O'Shea KS, Epstein JA. Neurofibromin deficiency in mice causes exencephaly and is a modifier for Splotch neural tube defects. Dev Biol 1999;212:80–92.
42. Pinto SS, Gottfried C, Mendez A, et al. Immunocontent and secretion of S100B in astrocyte cultures from different brain regions in relation to morphology. FEBS Lett 2000;486:203–7.
43. Zschocke J, Bayatti N, Clement AM, et al. Differential promotion of glutamate transporter expression and function by glucocorticoids in astrocytes from various brain regions. J Biol Chem 2005;280:34924–32.
44. Won CL, Oh YS. cAMP-induced stellation in primary astrocyte cultures with regional heterogeneity. Brain Res 2000;887:250–8.
45. Peters JL, Earnest BJ, Tjalkens RB, Cassone VM, Zoran MJ. Modulation of intercellular calcium signaling by melatonin in avian and mammalian astrocytes is brain region-specific. J Comp Neurol 2005;493:370–80.
46. Wink MR, Braganhol E, Tamajusuku AS, et al. Extracellular adenine nucleotides metabolism in astrocyte cultures from different brain regions. Neurochem Int 2003;43:621–8.
47. Kimelberg HK, Goderie SK, Conley PA, et al. Uptake of [^{3}H]serotonin and [^{3}H]glutamate by primary astrocyte cultures. I. Effects of different sera and time in culture. Glia 1992;6:1–8.
48. Horiguchi S, Takahashi J, Kishi Y, et al. Neural precursor cells derived from human embryonic brain retain regional specificity. J Neurosci Res 2004;75:817–24.